AD_____

AWARD NUMBER: W81XWH-04-2-0022

TITLE: Development of a Multileaf Collimator for Proton Radiotherapy

PRINCIPAL INVESTIGATOR: James McDonough, Ph.D.
Steven Avery, Ph.D.
Peter Bloch, Ph.D.
Dickson Goulart, Ph.D.
Mark Ingram
Richard Maugham, Ph.D.
James Metz, M.D.
Joshua Scheuermann
Zelig Tochner, M.D.
Arnaud Belard
Dan Fry, Ph.D.
John O'Connell, M.D.
Wilfred Sewchand, Sc.D.

CONTRACTING ORGANIZATION: University of Pennsylvania
Philadelphia Pennsylvania 19104-6205

REPORT DATE: June 2006

TYPE OF REPORT: Annual

PREPARED FOR: U.S. Army Medical Research and Materiel Command
Fort Detrick, Maryland 21702-5012

REPORT DOCUMENTATION PAGE

Form Approved
OMB No. 0704-0188

1. REPORT DATE *(DD-MM-YYYY)*	**2. REPORT TYPE**	**3. DATES COVERED** *(From - To)*
01-06-2006	Annual	17 May 05 – 16 May 06

4. TITLE AND SUBTITLE

Development of a Multileaf Collimator for Proton Radiotherapy

5a. CONTRACT NUMBER

5b. GRANT NUMBER
W81XWH-04-2-0022

5c. PROGRAM ELEMENT NUMBER

6. AUTHOR(S)
James McDonough, Ph.D., Steven Avery, Ph.D., Peter Bloch, Ph.D., et al.

E-Mail: mcdonough@xrt.upenn.edu

5d. PROJECT NUMBER

5e. TASK NUMBER

5f. WORK UNIT NUMBER

7. PERFORMING ORGANIZATION NAME(S) AND ADDRESS(ES)

University of Pennsylvania
Philadelphia Pennsylvania 19104-6205

8. PERFORMING ORGANIZATION REPORT NUMBER

9. SPONSORING / MONITORING AGENCY NAME(S) AND ADDRESS(ES)
U.S. Army Medical Research and Materiel Command
Fort Detrick, Maryland 21702-5012

10. SPONSOR/MONITOR'S ACRONYM(S)

11. SPONSOR/MONITOR'S REPORT NUMBER(S)

12. DISTRIBUTION / AVAILABILITY STATEMENT
Approved for Public Release; Distribution Unlimited

13. SUPPLEMENTARY NOTES

14. ABSTRACT

This report describes the second year of a project to design and construct multileaf collimators (MLC) to be used in proton radiotherapy, and the first year of the project to develop scanned beam technology for proton radiotherapy. This research project is a joint collaborative effort between the University of Pennsylvania (HUP) and the Walter Reed Army Medical Center (WRAMC) and is part of a larger project to build a state-of-the-art proton radiotherapy facility in Philadelphia in collaboration with the Children's Hospital of Philadelphia (CHOP). The accomplishments during the past year of the project are described in this report. (1) We developed software to read in DICOM-RT datasets and convert them to the GEANT4 geometry structure so we can calculate dose and display DVHs on CT data, (2) We incorporated a realistic proton nozzle into the GEANT4 Monte Carlo, (3) We started the study of spot-scanning optimization and have implemented two algorithms so far, and (4) The WRAMC group has started studying how heterogeneities affect the dose distribution in proton therapy.

15. SUBJECT TERMS
Radiation Oncology, Proton Therapy, Multileaf Collimator, MLC, Conformal Radiotherapy

16. SECURITY CLASSIFICATION OF:			**17. LIMITATION OF ABSTRACT**	**18. NUMBER OF PAGES**	**19a. NAME OF RESPONSIBLE PERSON**
a. REPORT	**b. ABSTRACT**	**c. THIS PAGE**			**19b. TELEPHONE NUMBER** *(include area code)*
U	U	U	UU	30	USAMRMC

Table of Contents

Introduction

The overall goal of this multi-year research project in collaboration with the Walter Reed Army Medical Center is to develop the necessary tools to make the proton facility that is to be constructed in Philadelphia the most advanced proton radiotherapy center. The first tool is the development of a multileaf collimator (MLC) for proton therapy and investigates the issues that must be resolved to use an MLC in proton therapy. The second tool under study is the optimization of the spot-scanning delivery technique including the effects of organ motion. This report describes the progress during the second year of the expected five year process. Included in that progress are the following activities and achievements: (1) Adaptation of the GEANT4 code to read in DICOM-RT data so structures and beams could be transferred between a treatment planning system and the Monte Carlo program, (2) Conversion of a CT dataset to a series of materials with densities so the Monte Carlo could accurately calculate doses on CT slices and construct DVHs from that data, (3) Incorporated a realistic proton therapy nozzle, including modulator wheel and scattering system, into GEANT4, (4) Began work on optimizing the spot-scanning delivery method including a comparison of optimization algorithms and studying the effect of the distance between spots on the flatness of the resulting dose distribution. A related effort, not included in the research project, has been to select a vendor for the proton therapy facility that will become import in the next year of the MLC project since the next steps are to design and build a prototype device.

Body

Together, the Hospital of the University of Pennsylvania (HUP) and The Children's Hospital of Philadelphia (CHOP) are building the most advanced cancer treatment facility in the world. This will be a fully-integrated facility utilizing state-of-the-art imaging and conformal treatment techniques for both conventional x-ray therapy and proton beam therapy. The project involves close collaboration between the HUP and CHOP. HUP is planning to build its Center for Advanced Medicine (CAM) on a site that will now include a proton therapy facility. This is a change that occurred since last year when the plan was to build the proton portion of the facility on CHOP property. That change was made for several reason; among them was the difficulty of integrating a facility owned by two different entities. Overall the new design is much better from a construction and operating point of view. CHOP will still maintain a financial stake in the facility but it will be a smaller fraction than projected last year when CHOP would have a majority stake.

A project of this size and scope requires careful planning and a key issue is equipment selection. In the report last year we indicated that the number of vendors under consideration was reduced to three. During the past year HUP has signed a letter of intent with one of those vendors and has initiated contract negotiations with them. The current timescale to finalize the contract is summer of 2006. Because the design and construction of the building is required prior to the installation of equipment, it will become the critical step in the project once the agreement is signed so the design portion has already been initiated under the assumption that the vendor will in fact be the one with whom the negotiations are presently taking place. We expect that this parallel design and contact negotiation will save six months on the schedule and will allow for first patient treatments in the fall of 2009.

The rationale for the overall proton project lays in the fact that proton beams offer highly significant advantages over x-rays in the sparing of normal tissues. This is due to the physical characteristics of the proton beam compared to x-rays. X-rays are electromagnetic waves that are highly penetrating, and will deliver dose throughout any volume of tissue irradiated, regardless of thickness. Thus x-rays always deliver substantial doses of irradiation both proximal and distal to the tumor volume. Furthermore, even for the most energetic x-ray beams available for practice, the depth at which the maximum dose of radiation is delivered (D_{max}) ranges from as little as 0.5 cm to a maximum of 3 cm depending on the energy utilized. Because a tumor is almost always located deeper than these ranges, a higher dose is invariably delivered to the normal tissues proximal to the tumor, and the tumor is always treated in the region of the beam where the energy deposition is falling off. To some extent this can be overcome by bringing in beams from multiple directions, centered on the tumor, allowing the dose to sum within the tumor volume. However, since the beam travels throughout the entire thickness of the body, all normal tissues from the entrance area to the exit of the beam will be affected.

Unlike with x-rays, the absorbed dose of a proton beam increases very gradually with increasing depth and then suddenly rises to a peak at the end of a proton range. This is known as the Bragg Peak (Fig. 1). A proton beam can be directed so that the Bragg Peak occurs precisely within the tumor volume, something that can almost never be done with x-rays. The dose around the tumor volume is much less than the tumor itself, thus sparing the normal tissue in this area. The dose immediately beyond the Bragg Peak of a proton beam is essentially zero which allows for the sparing of all normal tissues beyond the tumor volume. Side effects, both acute and long-term, typically seen with x-ray therapy can thus be markedly reduced with proton beams by sparing

normal tissues that are situated around the tumor. These considerations are directly related to the physical characteristics of the proton beam, and require no demonstration or study. Initial clinical studies demonstrate the efficacy of proton therapy. It should be remembered however that the available clinical data are somewhat limited because most proton facilities have treated only a limited number of patients.

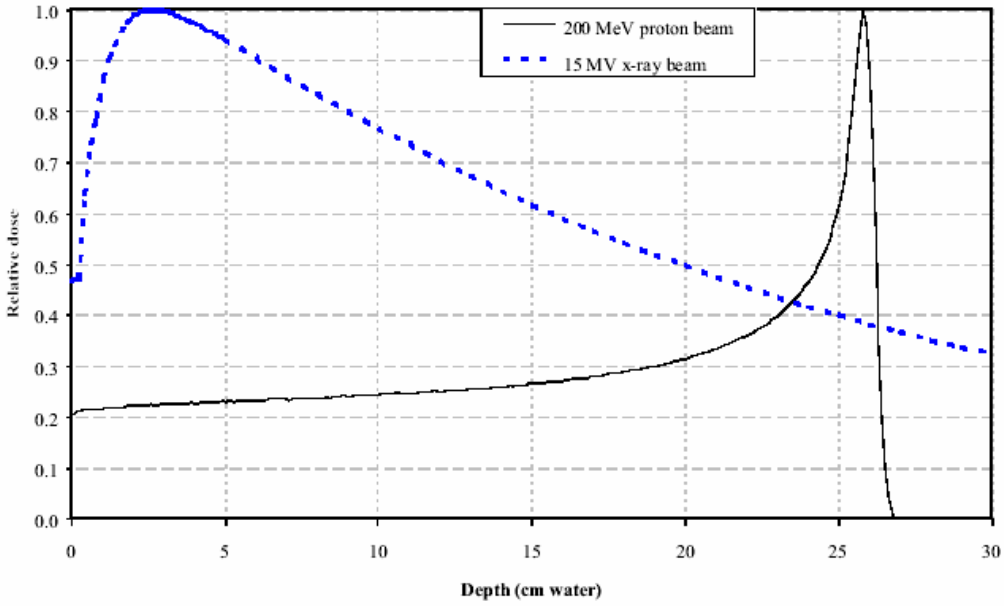

Fig. 1. Comparison of the relative depth dose for proton and x-ray beams.

A number of published studies[1-6] have documented the clinical advantages of proton beams, and shown decreased normal tissue toxicity, compared to conventional photons. Numerous sites within the body have been shown to be more effectively treated with proton beam therapy. By limiting the dose to normal structures, higher doses can safely be delivered to the tumor itself. This should result in higher local control and ultimately increased survival while minimizing side effects of therapy.

The treatment of pediatric tumors with proton therapy provides a unique opportunity to significantly reduce the acute and long-term complications associated with conventional radiation therapy. The pediatric population is exquisitely sensitive to the effects of radiation therapy. Long-term sequelae including growth abnormalities, second malignancies, neurologic complications, cardiac and pulmonary toxicities, and infertility may all be reduced with the use of proton therapy. X-ray therapy causes effects on the hearts and lungs of pediatric patients, again due to the problem of "exit" dose. A study of long-term survivors of children treated with x-rays to the spinal axis showed that 31% had abnormal EKGs and 75% had reduced exercise capacity. Jakacki et al.[7] reported that 60% of patients treated to the spine showed restrictive lung disease. Proton beams should be able to entirely avoid these complications since the uninvolved normal structures can be totally avoided.

The research element of the proton facility has brought together the expertise of HUP and WRMAC to initially identify five projects, to be started over a period of five years, that will

result in the technology and protocols to make the new center the most advanced cancer treatment facility in the world. Each of these projects will help advance proton therapy worldwide and result in measurable benefits. The five projects are as follows:

(1) Multi-leaf collimator (MLC) for use on proton therapy gantries

(2) Cone Beam CT on the Gantry for localization of target volumes

(3) Proton Radiography to determine dose and stopping power of various tissues

(4) Positron Emission Tomography (PET) imaging on the gantry to evaluate dose deposition within tissues irradiated

(5) Scanning proton beam using adaptive radiotherapy techniques based on implementation of MLC, Cone Beam CT, PET imaging.

This report concentrates on the second year achievements of the multileaf collimator design and development project and the first year of work on the spot-scanning/motion project.

The Statement of Work in the approved grant proposals included the following items to be investigated during the first two years for the MLC development and the first year of the spot-scanning development:

MLC Development

1. Leaf design: The specification of the leaf material and shape will be determined so the final design will: (1) reduce to permitted levels the leakage of radiation through the MLC onto the patient; and (2) keep the activation of the MLC, and consequently the exposure to our radiation workers, to as low a level as can reasonably be achieved. This work will be performed in consultation with our chosen vendor using a combination of published literature and Monte Carlo simulations. (Year 1)

2. Joint Military/Civilian Proton Radiotherapy Center: The oversight and management for this research will be coordinated through a Joint Military and Civilian Proton Radiotherapy Center to be established at Walter Reed Army Medical Center. Approximately 5% of the total funding will be necessary for renovation of space at WRAMC to create this center. This center is necessary to provide working space for the project administrator and scientific writer. This Center will also serve as the hub through which the Walter Reed investigators will conduct their research on this proposal. In addition to the oversight and management to be provided through this center and the research performed by the Walter Reed investigators in this Center, a third purpose of this center will be life cycle management of the Center in order to secure continual funding to guarantee this Center is transformed into the remote treatment planning and management clinic envisioned in the preface [of the grant proposal]. (Years 1-2)

3. Investigate the design factors affecting the lateral penumbra of the beam: The quality of the dose distribution from a proton beam, particularly the lateral penumbra, directly depends on the distance between the final collimator and the patient surface. Ideally we want the MLC as close as possible, but that may limit the ability to rotate the gantry

around the patient. A compromise solution will be determined using Monte Carlo simulation to study how the position of the MLC affects the lateral penumbra. (Year 1)

4. Design of the MLC system: The electromechanical design and assembly of the MLC will be done in consultation with the chosen vendor. The leaf drive mechanism must be designed to minimize the overall dimensions of the collimator. A high-precision leaf position setting and verification system must be designed. The mechanism for mounting the collimator assembly on the proton beam delivery nozzle must be designed to avoid patient-collimator interference problems and be adaptable to the specific requirements for treating a wide range of anatomical sites. A suitable computer-based control system will be designed, which will allow for the treatment of individual fields as a series of multiple segments. We expect to take advantage of the experience gained from the manufacturers of x-ray MLCs. (Year 1)

5. Production of a prototype MLCs and initial testing: The vendor will produce a prototype MLC based on the design determined above. The various components will be tested and modified if necessary. (Year 2)

6. Incorporation of the MLC design into the treatment planning system: The vendor of the treatment planning system (TPS) will provide software to incorporate MLCs based on the design determined above. This software will have the ability to export the MLC pattern to a record-and-verify system and will account for any limitations on the positioning of the leaves. (Year 2)

Spot-Scanning development

1. Scan optimization: The quality of the scanned proton beam dose distribution, particularly the beam uniformity, the beam lateral penumbra and the Bragg peak distal edge dose fall-off, depend on the pencil beam size and the placement of the individual pencil beams or beam spots. A Monte Carlo simulation will be used to model the beam dose distribution and study the sensitivity of the beam uniformity, lateral penumbra and Bragg peak distal fall-off to the pencil beam size and placement. The effect of beam size and placement patterns on the overall dose delivery time will also be investigated. The simulation studies will assist in designing scan patterns and software control systems for the scanned beam (Year 1).

2. Patient motion simulation: The effects of patient motion will also be modeled using the Monte Carlo simulation. The effects of repeatedly scanning the treatment volume, commonly termed over scanning or repainting, will be investigated and the ability of this technique to produce acceptable uniform dose distributions within the treatment volume will be assessed. Other methods of conforming the dose to the treatment volume in moving targets, including beam gating, breath hold a tumor tracking will be similarly assessed. The impact of the various methods proposed for overcoming organ/tumor motion on overall treatment time will be studied. (Years 1-2).

Progress

The work over the last year can be broken into three areas relating to: (I) MLC development, (II) spot-scanning development and (III) work at Walter Reed as a subcontractor and collaborator.

I. MLC progress

a. Importing Dicom-RT CT Image Sets into Geant4 Environment

Introduction

CT Images consist of a voxelized region of the patient chosen at the time of the scan. The image set consists of one or more 2-dimensional images at different locations along the patient's body, i.e. slices. The voxel size and slice thickness can be adjusted and determine the resolution. Each voxel is assigned a CT Number, in Hounsfield units, which is a measure of the linear attenuation of the material in that voxel. The Hounsfield unit is a comparison of the linear attenuation coefficient of some material to that of water.

The Digital Imaging and Communications in Medicine (Dicom) Standard gives a set of guidelines for the storage and transmission of Digital Image files. The standard provides a framework for encoding and decoding digital images. A basic CT Image is a binary file consisting of a header, which contains relevant patient and scan information, and the data, which is a sequential listing of the Hounsfield units of each voxel.

The Dicom Standard was then furthered to include various RadioTherapy Extensions, called Dicom-RT. Most importantly for this project, Dicom-RT includes standards for the encoding clinical structures and treatment plans in RTStruct and RTPlan files respectively.

This project had five major phases: 1.) Learn about the Dicom Standard and become familiar with the Geant4 environment,[8] 2.) Import a CT-Image Set into the Geant4 environment as a "Phantom", 3.) Read in the Structures and be able to "apply them to the images", 4.) Determine the energy deposited in each voxel/structure to eventually generate DVH curves, 5.) Read in Plan data so as to simulate a multibeam treatment.

The DICOM Format

Basically the Dicom standard is a set of codes that define different types of data. A piece of data in a Dicom file is defined by four pieces of information. The first piece is the attribute tag which is a 4-byte code that defines the type of data being defined. This tag is followed by a value representation code, which is a 2 byte code that tells the type of data to follow, i.e decimal string, short, etc.. The value representation also defines the length of the next part of the data. The third piece of data is the value length, which is a 2 or 4 byte unsigned integer that defines the length of the piece of data. The final piece is the value, or data, itself. A single piece of data has the form:

GroupID	ElementID	ValueRep	ValueLength	Value

GroupID and ElementID are each 2-btye portions of the attribute tag, combine tey make up the entire tag. A Dicom file is a binary file with data encoded in the above format one right after the other.

Importing CT-Images into Geant4

A DICOM example was provided with Geant4. This DICOM example provided code that was supposed to read in a CT Data Set and create a Parameterized phantom from the CT Data. The code did not initially compile and there were problems with it that kept it from initially working with Data from the CT Scanner at HUP. The structure of the program however was fine.

The CT Images are initially decoded; first the header is read and the relevant parameters (i.e. slice location, number of rows, number of columns, voxel size, etc.), then the Data is read. The Data is converted from Hounsfield units to Physical Density (Fig. I.1). The relevant header information and the converted Data are written to an ASCII file for later access by the methods that will create the phantom.

The CT image set defines a 3D grid of size Number of Rows by Number of Columns by Number of Slices. The size of each voxel in the grid is X Pixel Spacing by Y Pixel Spacing by Slice Thickness. Using a parameterization, the program goes through each voxel in the CT set and determines the material and position of the voxel and places it in the phantom. Fig. I.2 shows the identification of anatomical composition derived from the Hounsfield number.

Read in the RT Structures

The Structure file has a format very similar to the format for a CT image. It is also a binary file, however it utilizes sequences, or nested data sets. The sequences allow for the repetition attribute tags through out the file. For example (3006,0050) signifies contour data. This tag will be repeated through out the Structure file for each contour, however, the other data members of the sequence will define what the contour is and where it is from. Nested within each sequence is the name of the contour and the slice on which it belongs. This allows for relatively easy storage of the contours.

One hurdle that had to be overcome with the contours is that they are defined in the “CT Scanner frame of reference.” This frame of reference is defined by the position of the upper left hand corner of the CT Image. However, the phantom was being placed in the center of the world created in Geant4, so the contours have to be shifted to coincide with the “GEANT Frame of Reference.”

The contours allowed for a simplification of the geometry. A majority of the CT images are empty or just air. So, by reading in the contours and finding the external contour, just the voxels that are part of the patient can be read in. This means that the number of “active” voxels was greatly reduced. Any voxels that were not within the external contour were just set to air. Reading in the structures allowed for the generation of DVHs.

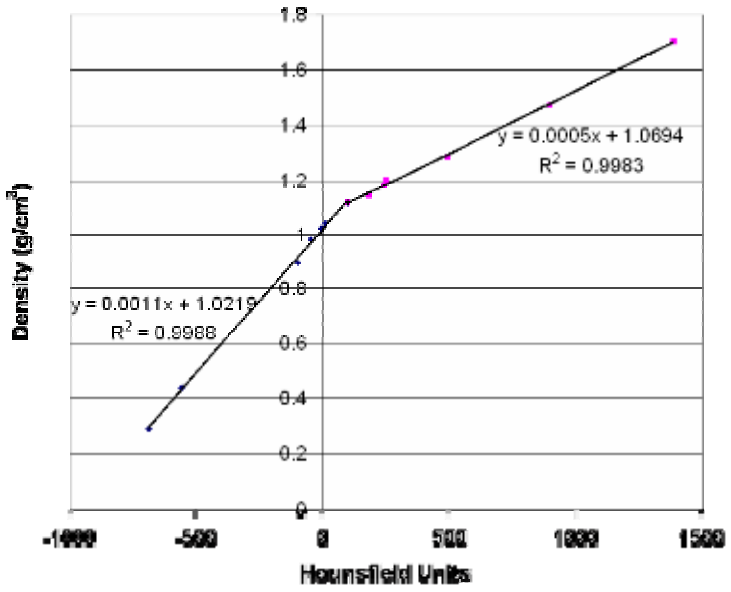

Fig. I.1. Relationship between density and CT number.

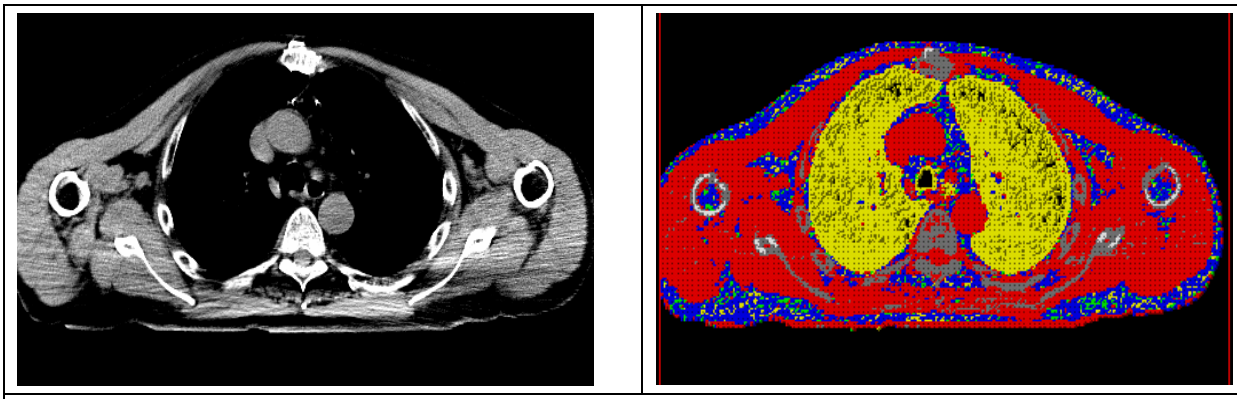

Fig. I.2. Construction of material composition of anatomy derived from CT number.

Reading in the RT-Plan File

The format of the RT-Plan file is exactly the same as the structures file. Currently the only parameters that are read in are the number of beams, the angles of the beams, their energies and isocenter. Isocenter for the beam is the center of the world in Geant4, so the phantom was shifted so that isocenter in the patient was in the center of the world. This meant that the contours again had to be shifted to account for isocenter. Reading in the Plan file allowed for the simulation of an external beam treatment.

Generation of Dose Volume Histograms

Once dose has been calculated on a voxel-by-voxel basis and the voxels have been assigned to the proper structures, we can then create dose-volume-histograms (DVH).

The DVHs are a primary tool used by radiation oncologists to determine the suitability of a treatment plan.

b. Interface Effects using Geant 4

Our colleagues at Walter Reed reported findings concerning the effects of a proton beam at a water-bone interface. Their results showed that when 1 cm of bone was placed in the path of 150 MeV proton beam a large upward spike in dose occurred right before the interface, followed by an equally large downward spike immediately after the water-bone interface. They also initially reported that the addition of bone had no effect on the position of the Bragg peak. These results seemed suspect, and we attempted to reproduce them.

The figure below shows the depth dose curve for a 150 MeV beam with 1 cm of bone and without the bone in a water phantom (red and blue respectively). No spike in dose was seen, and the Bragg peak does move shallower when bone is added, as is expected. The figure on the right displays the energy deposited, which is larger for bone because of its higher density.

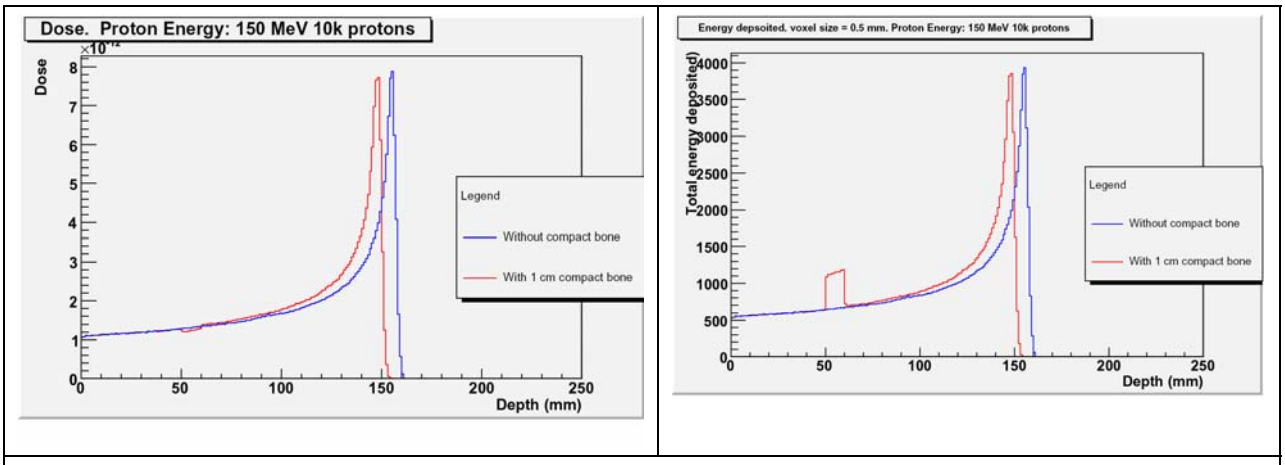

Fig. I.3. Dose (left) and energy deposited (right) with and without 1 cm of bone.

These results were passed along to our colleagues who determined that the apparent lack of shifting in the Bragg peak was due problems with their volume definitions. The presence of a spike is believed to be caused by the method with which they are storing particle information.

c. Modeling a realistic nozzle for double-scattered proton therapy

A major undertaking during the past year was to accurately model the devices in a proton nozzle for treatments using the double-scattering technique. In this type of proton beam delivery a proton passes through various materials in ways that vary from vendor to vendor. We signed a non-disclosure agreement with one of the vendors so that we could have access to their detailed nozzle design. For this design (see Fig. I.4) protons pass through (1) a first scattering foil to begin spreading out the beam in a Gaussian distribution, (2) one of nine possible modulator wheels that cause the dose deposited in the patient to spread in the depth direction, (3) a second scatterer that rescatters the

central portion of the beam to form a beam that will deposit dose uniformly in the direction perpendicular to the direction of the proton, (4) a set of collimators to remove beam outside the lateral extent that we require, (5) the MLC (or aperture) that shapes the beam to the size that we need, and (6) a phantom in which we measure the resulting dose. One component not included yet is the bolus or compensator, which shapes the distal part of the dose distribution.

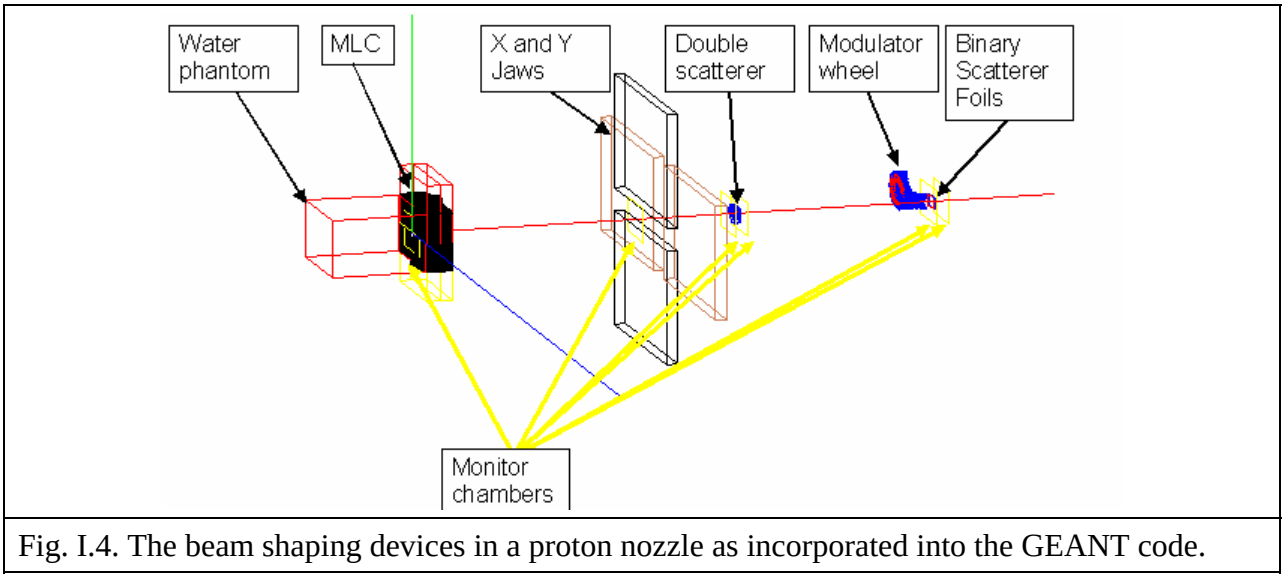

Fig. I.4. The beam shaping devices in a proton nozzle as incorporated into the GEANT code.

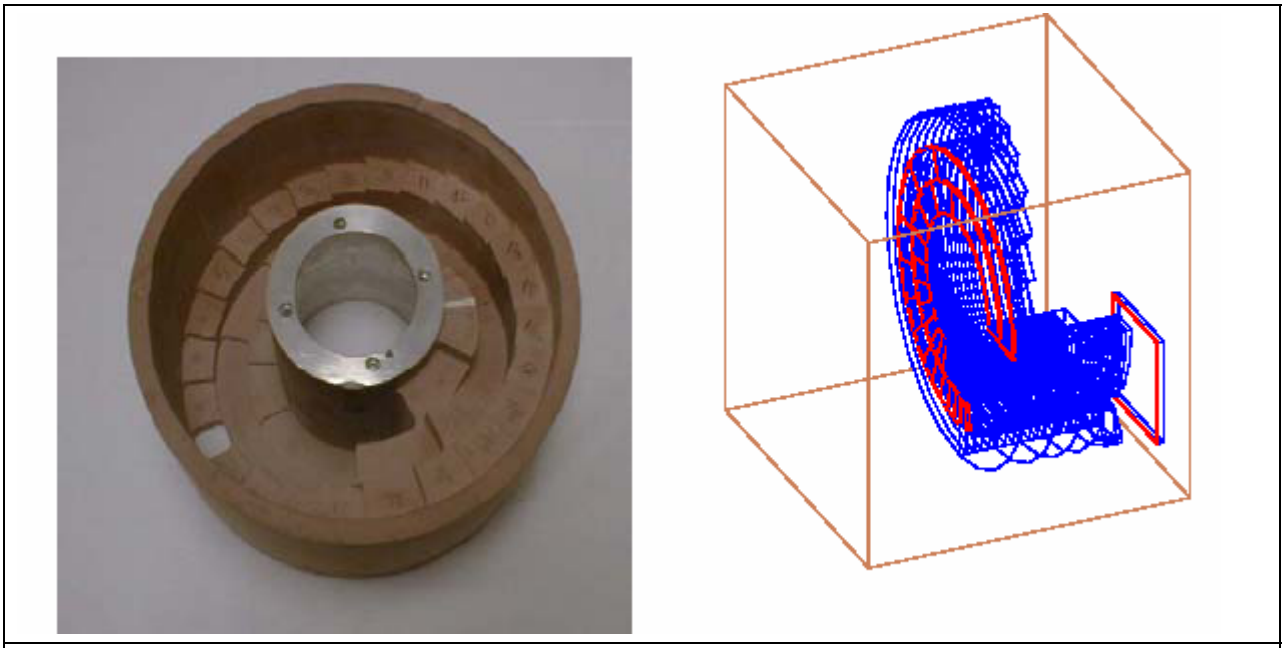

Fig. I.5. A photograph, and the GEANT4 representation, of one modulator wheel with three separate tracks to generate different spread-out Bragg peaks.

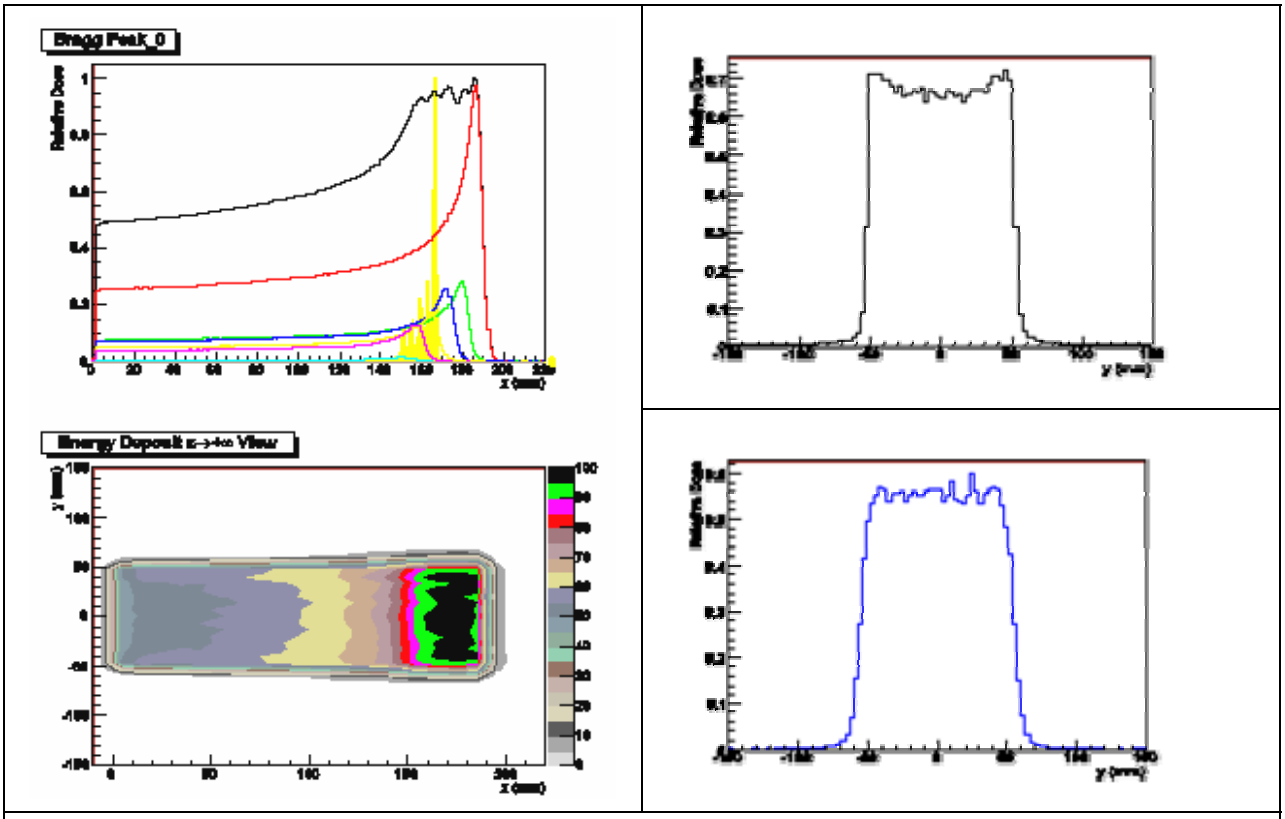

Fig. I.6. Resulting dose distributions using the proton nozzle elements shown in Fig. I.4. On the top left, the energy of the protons is shown for the total and for the ones that exit each step of the modulator wheel. On the bottom left is a two-dimensional dose distribution and on the right are the two view in the direction perpendicular to beam direction.

II. Spot-scanning progress

a. Spot-Scanning Studies in a Geant4 Environment

Spot position and weights

There are two different approaches to scanning a particle therapy beam. The most common method, called spot-scanning or step-and-shoot, positioned the beam using magnets to a specific spot and stays there until a specified amount of beam is delivered. The second method, called raster-scanning, continuously sweeps the beam across an area while modulating the beam current so more or less dose is delivered to specific areas. The easier method to implement, and the one most commonly used, is the spot-scanning technique. It has one disadvantage compare to raster-scanning in that the time to move the beam from spot to spot can become quite large.

The focus of the initial year of our project is to reduce the treatment time by optimizing the delivery of the spots. In Fig. II.1 a simple example of a treatment volume (CTV) and a surrounding region (rind) is shown. The purpose of the rind is to assure that the CTV reaches the correct dose even if some region outside receives dose. Spot positions are predetermined and are allowed to be in the CTV or the rind but nowhere else.

The steps in calculating the spot-scanning pattern are: (1) use GEANT4 to calculate the dose to each voxel per proton from each spot; (2) truncate the resulting dose distribution so that voxels with little or no dose are excluded, (3) find the number of protons needed at each spot so that the dose distribution satisfies the clinical constraints, and (4) use the initially calculated dose-per-voxel per proton and the number of protons to generate a final dose distribution and DVH (Fig.II.2).

Using these steps repeatedly we can understand the effect of eliminating low-weight spots and, in the next stage of this project, what effect organ motion has on the resulting dose distribution and how we can minimize it.

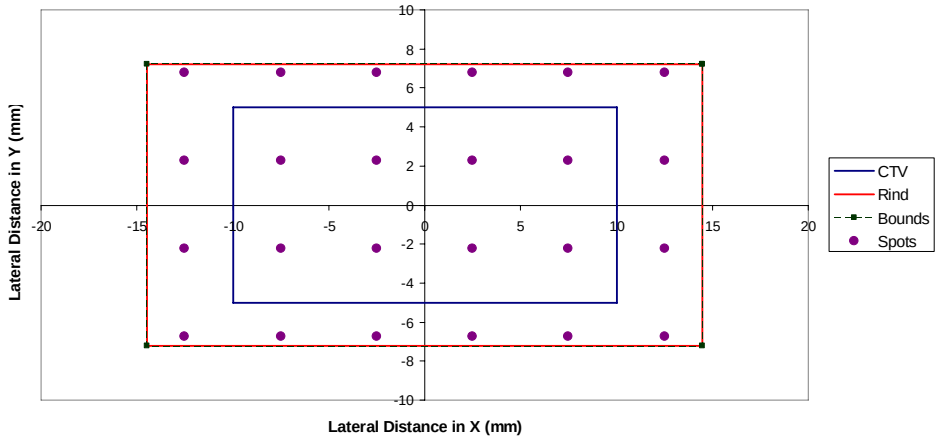

Fig. II.1. Example of a spot pattern to cover a CTV, some spots are indicated as falling outside the CTV but inside a “rind”. The optimization algorithm will determine the weights for each spot.

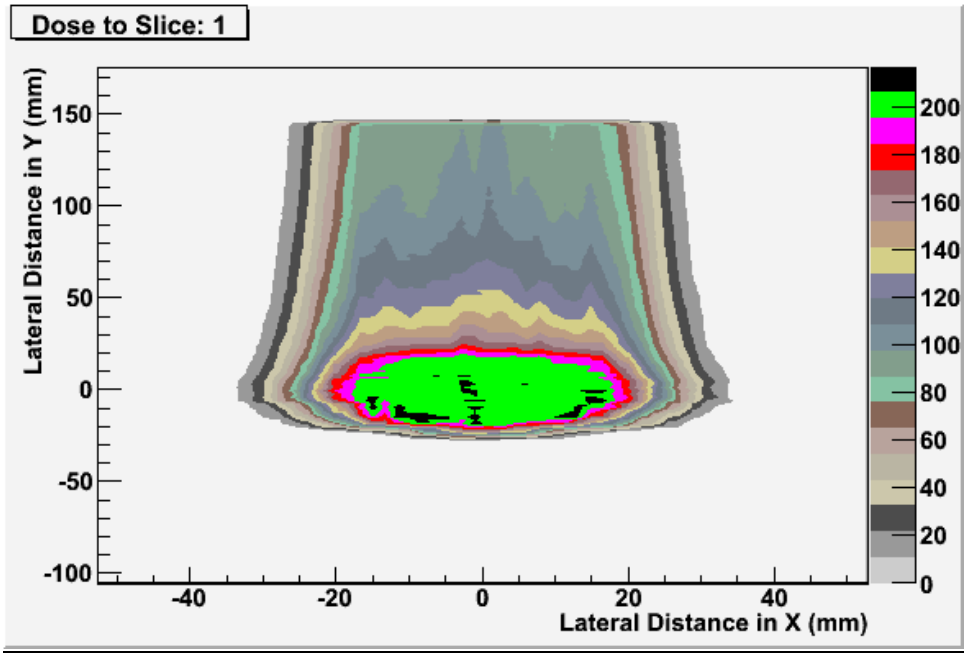

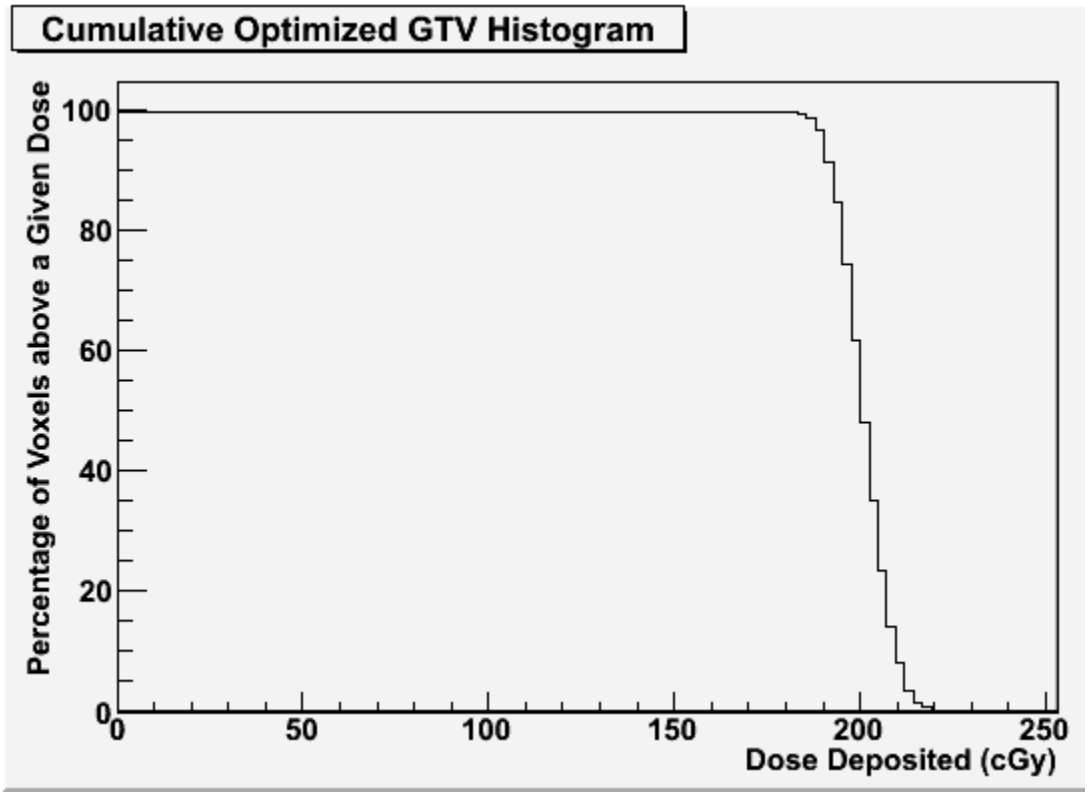

Fig. II.2. Resulting dose distribution and DVH from an optimization of the scanning pattern shown in Fig. II.1.

Comparison of optimization methods

An algorithm must be used to find the number of protons (or weights) per spot (step 3 above). Generally one uses an optimization algorithm that attempts to find the "best" solution. Alternatively one can use a "feasibility" algorithm that attempts to find a satisfactory solution that may not be the "best". The advantage of the latter approach is that it can be much faster.

A feasibility algorithm that has recently been applied to radiotherapy is the Cimmino approach.[9] The fact that this algorithm finds a solution for a series of inequalities makes it ideal for a field where we always want doses to critical structures to be "less than" some amount and for doses to targets to be within a narrow range.

In addition to optimizing beam weights using the Cimmino Algorithm we also deemed it beneficial to use a more traditional optimization method. This method will allow us to compare the results from Cimmino with an algorithm that is both more familiar and understandable.

We developed a gradient method in the form of a steepest descent method. Although computationally inefficient, the method appears to always converge. The steepest descent method utilizes as input the same $m \times n$ dose vector as Cimmino (m being the number of voxels and n the number of beams or "spots") and outputs optimal beam weights to obtain a desired solution. The function which we desire to minimize by the algorithm is

$$\left((DX - P)^2 W \right)^{1/2} \qquad (1)$$

where D is our dose vector($m \times n$), X (n dimensions) P (m dimensions) is our prescription or target dose to each voxel and W(m dimensions) is the weight or relative importance of each voxel. In order to more closely match the Cimmino algorithm we provide a maximum and minimum dose to each voxel where the difference $(DX-P)_m$ is set to zero if the actual dose is between the max and min prescriptions.

The beam weight vector X is seeded with some initial value and an n dimensional gradient vector G is then calculated. Derivatives are approximated using the midpoint method. By moving in the opposite direction of the gradient we are assured to be moving in the direction of steepest descent of the function (equation 1). The algorithm next performs a line minimization which roughly determines what size step in the direction of the steepest descent provides the smallest value for equation 1. This step is then taken, and the algorithm repeats until it converges. Currently, convergence is defined to be when the percent difference between a given interval of steps is sufficiently small. Initial comparisons between Cimmino and the gradient algorithm indicate that both methods give extremely similar results, as seen in the figures below.

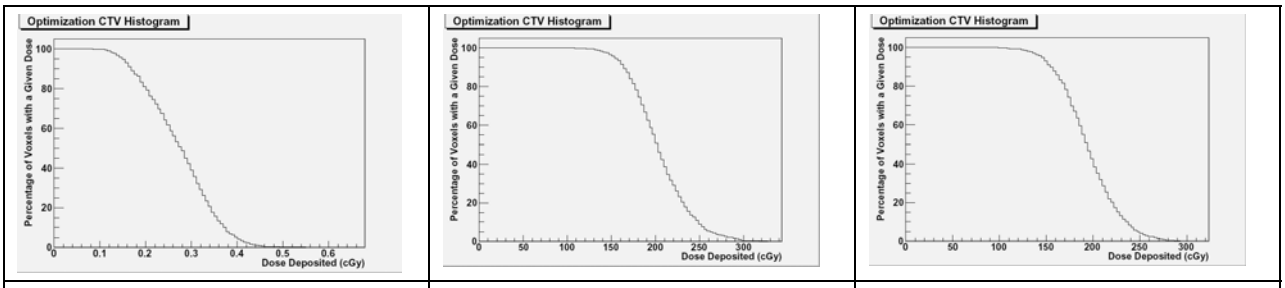

A) Pre-optimized	B) Cimmino	C) Gradient method

Fig. II.3. DVH of CTV for treatment of 24x14x18 mm target volume. Shown for (a) Pre-optimization, (b) optimization using Cimmino algorithm, and (c) Gradient method. Spot size is 8 mm FWHM and spacing between spots is 1 FWHM, with spacing in the beam direction being 4.5 mm. Target volume is a water phantom inside a larger water phantom. Beam is in the y direction. Energies are 115 MeV.

The Cimmino method converges several times faster than the gradient method, as is to be expected. Also noted was that Cimmino will set beam weights to zero where the gradient method will set them to very low values but not zero. The similarities in the dose distributions are seen in the following transverse plane slices.

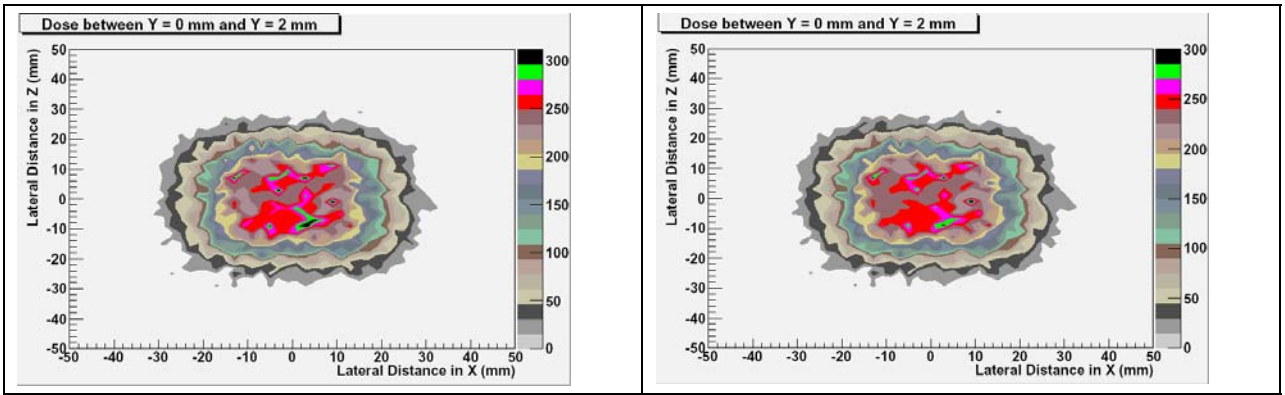

Fig. II.4. Comparison of the dose distributions from optimizations using the Cimmino algorithm (left), and the Gradient method (right). Conditions are the same as in Fig. II.3.

Spacing of Spots

Another issue that was addressed was that of spot spacing. In order to determine what spacing would give adequate dose uniformity we began by simply adding adjacent Gaussians and calculating the percent difference between the maximum and minimum within the central region. The figures below illustrate how the spacing of Gaussians at different intervals affects uniformity. The percent difference of the max and min as a function of spacing (in terms of FWHM) was then calculated for the 1-D case, as well as the 2-D case with the spots staggered. Based on these calculations, we believe that a spot

spacing of 0.7 – 0.8 FWHM should cause sufficient dose uniformity. The issue of how the Gaussian distributions spread out with depth (the sigma dependence on depth) has not yet been addressed.

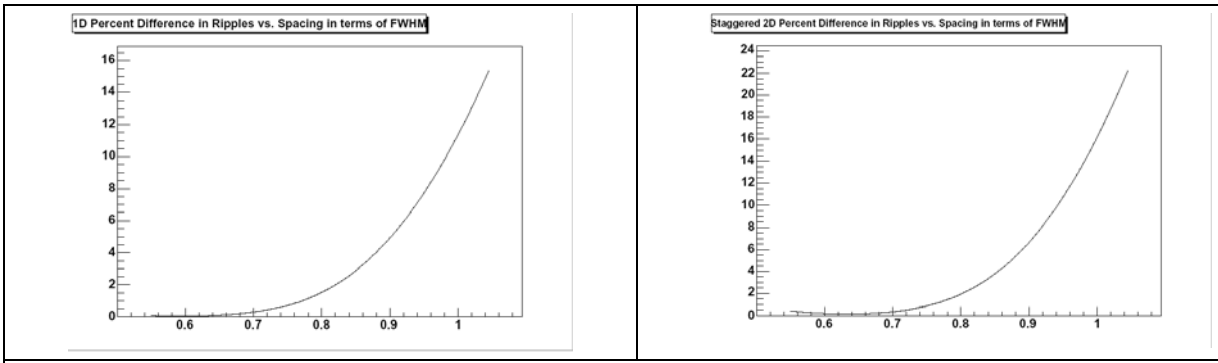

Fig. II.5. Percent difference between max and min as a function of spacing in terms of FWHM for 1-D (left) and 2-D (right).

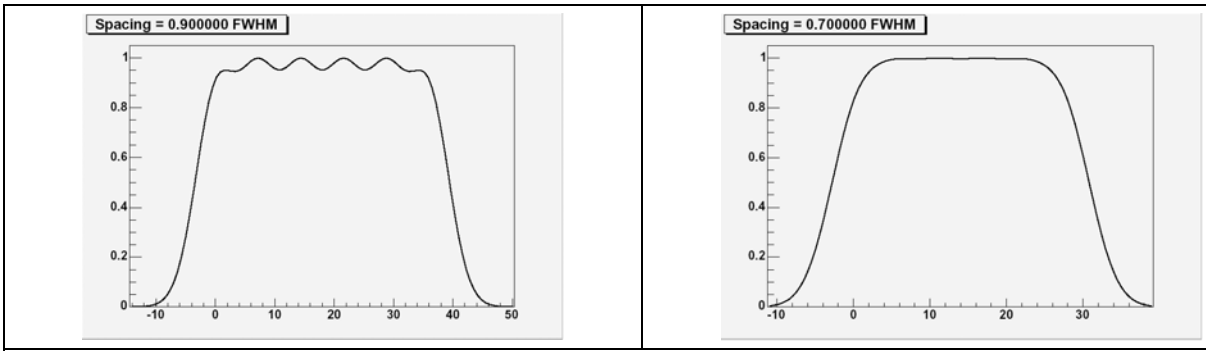

Fig. II.6. Overlapping Gaussian spots with spacing = 0.9 FWHM (left) and 0.7 FWHM (right)

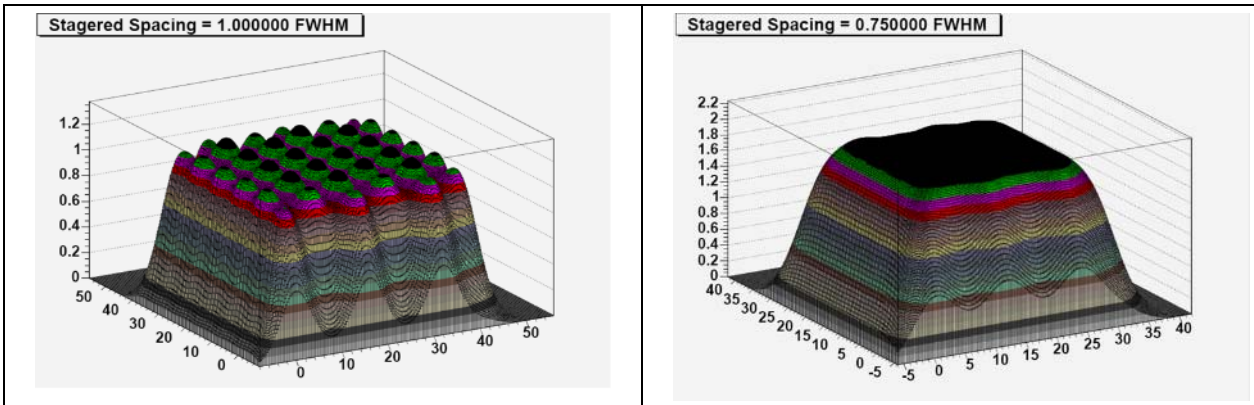

Fig. II.7. Overlapping Gaussian spots with spacing = 0.9 FWHM (left) and 0.7 FWHM (right)

III. Report from the Walter Reed Army Medical Center Group

Overview

Heterogeneities in the path of a proton beam are inevitable once the proton enters the human body. Treatment planning algorithms handle heterogeneous tissue and structures in a very simplified manner. In the absence of critical structures there is relatively good agreement between simplified treatment algorithms and Monte Carlo simulations. However, in the vicinity of critical structures errors in treatment planning algorithms can be quite large.

We have taken a rather different approach over past studies by simply looking at characterizing the effects of specific heterogeneities on the properties of the Bragg curve and lateral proton scattering. Monte Carlo routines are ideal in that we can easily simulate the deposited dose for a large host of configurations. As a result we have fortuitously identified a specific scaling relation that allows one to predict the shape of the Bragg distribution regardless of the material composition. As a point-by-point determination of material composition is obtainable for any patient via CT, we are now investigating the utility of the scaling relationships in predicting the dose distribution in and around complex heterogeneous structures.

Simulation Outline

All simulations were done with GEANT 4.7.0. Full 3d depth-dose distributions were simulated with 10^6 protons covering the entire therapeutic energy range of 70 MeV to 250 MeV. Run-to-run fluctuations were checked by performing several simulations at fixed energy for different random number seeds. Differences in extracted quantities were less than 1%. Mean energies of all primary and secondary particles, dose deposited by each particle, and type of interaction was recorded for post-simulation analysis. All materials have been modeled according to ICRU 49.

We are now running simulations on a 6-node, 12-processor Macintosh XServe G5 cluster with a total of ~50GHz processing speed. Run times have been reduced to roughly an hour or two for 10^6 protons, depending on the incident proton energy.

Key Results

We first investigated the material dependence of several key parameters characterizing the proton depth-dose distribution. These are shown in figure III.1. All simulations were performed on homogeneous materials "blocks" (referred to as phantoms) of different composition for 70 MeV – 250 MeV incident proton energy. Results are shown in figures III.2-III.5.

The key importance of the results is the *universal* scaling that exists over a large class of materials. Although not immediately apparent, the origin of the scaling variable x comes from the effective charge theories for heavy ions passing through stripper foils, where the mean charge state $\bar{q}$ of the exiting ions is expressed in terms of a reduced velocity

$$\bar{q} \propto (v/v_0)Z^{-\gamma}. \qquad (1)$$

In the above expression v is the incident ion velocity, v_0 is the Bohr velocity and Z_p the ion atomic number. We have simply inverted the problem by inverting the role of projectile and target atomic numbers Z_p and Z_t. In all studies here materials are compounds and Z_t must be defined as a sum over all constituent elements. The target atomic number is now expressed as an effective quantity, Z_{eff} where

$$Z_{eff} = \left(\sum_{i=1}^{N} a_i Z_i^{\,m} \right)^{1/m}$$
$$a_i = \left(\frac{N_{av} w_i}{A_i} \right) / \sum_{i=1}^{N} \frac{N_{av} w_i}{A_i} \quad . \qquad (2)$$

N_{av} is Avogadro's number, A_i the elemental atomic mass, and w_i the fraction by weight of each constituent element. The exponent has been taken to be the same as that used in photon irradiation $m = 2.94$. Expressing the proton velocity in terms of its energy E and using the effective Z of the compound from equation (2), the scaling variable used in figures 2-5 is

$$x = E^{1/2} \left(1836 E_0\right)^{-1/2} Z_{eff}^{\;\;-\gamma}. \qquad (3)$$

E_0 is the ground state energy of the electron in hydrogen. Note that the scaling exponent g is roughly 1/3 for the distal edge and FWHM but 1/4 for the lateral edge width. Qualitatively this would be expected since the physical interactions governing each is different, i.e. the distal edge and FWHM are dominated by energy straggling of the proton whereas the lateral edge is dominated by hard collisions between the proton and target (phantom material) nuclei. A more thorough physical explanation is currently being pursued.

In order to be useful in targets such as the human body, this scaling must be applicable in the presence of heterogeneities. We have begun investigations using a very simplified geometry but one that would have direct application to tumors such as glioblastomas. In this scenario the irradiating beam would pass first through the skull (bone) and then into soft tissue (water). Simulating a bi-phase system composed of bone and water should allow us to investigate the scaling validity in under more realistic conditions. The geometry layout is shown in figure III.6. The bone slab was taken to be compact bone with stochiometry defined in ICRU report 49.

To compare directly with the homogeneous phantom scaling results one must form the analogous effective atomic number of the heterogeneous water/bone complex. The most straightforward method is simply to sum the individual weights of Z_{eff} according to

$$\tilde{Z}_{eff} = \frac{1}{V} \sum_{j=1}^{n} v_i \left(Z_{eff} \right)_i , \qquad (4)$$

where v_i is the volume occupied by water (bone). The results are shown in figure III.7. The lateral edge results and FWHM results are similar. As a check of the "rigidity" of the scaling variable to changes in Z_{eff} we have also plotted in figure III.7 the distal edge results of the heterogeneous phantom but with either Z_{eff} of pure water or pure bone. As is seen the results do not scale unless we use the effective atomic number defined by equation (4). It is important to point out that even at the lowest incident proton energy simulated the Bragg peak was located sufficiently far from the bone slab, and thus there was no perturbation of the peak shape. Instead, the heterogeneity provided an additional "slowing down" mechanism that simply resulted in a shift in the Bragg peak to shallower depths. The breakdown in scaling due to perturbations of the peak is now under investigation.

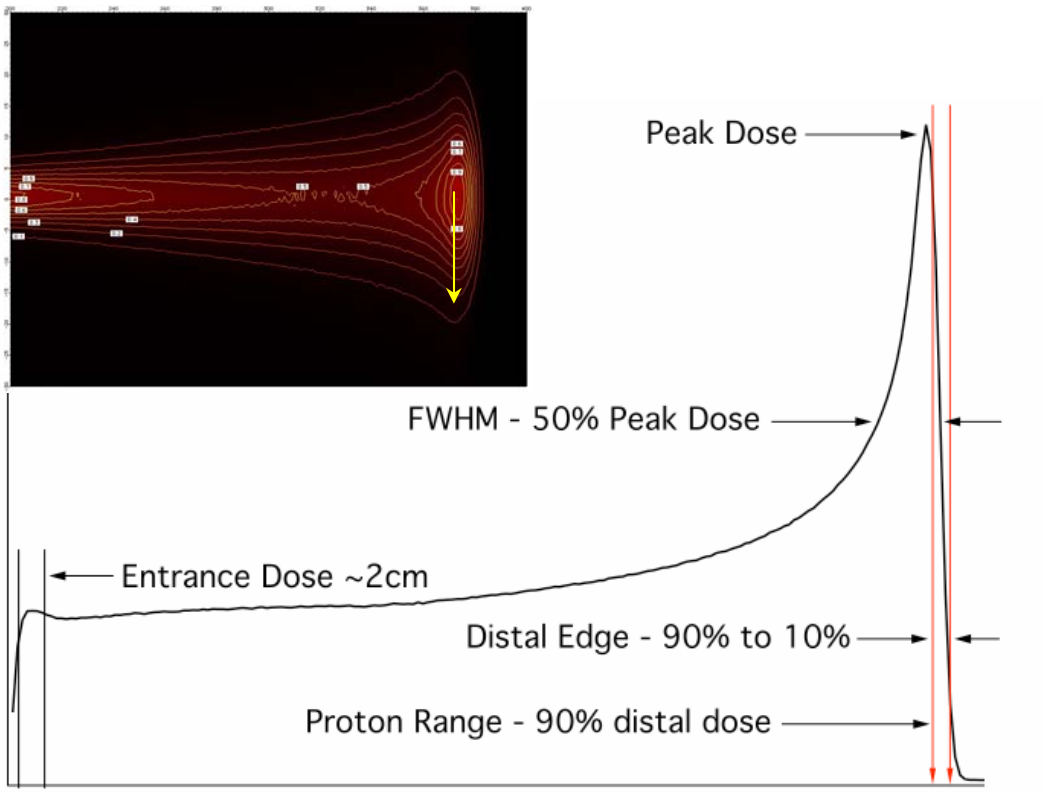

Figure III.1 Parameters used to characterize the axial % depth-dose. The lateral edge width (yellow line in inset) is defined analogous to the distal edge width in a plane perpendicular to the axial % depth-dose.

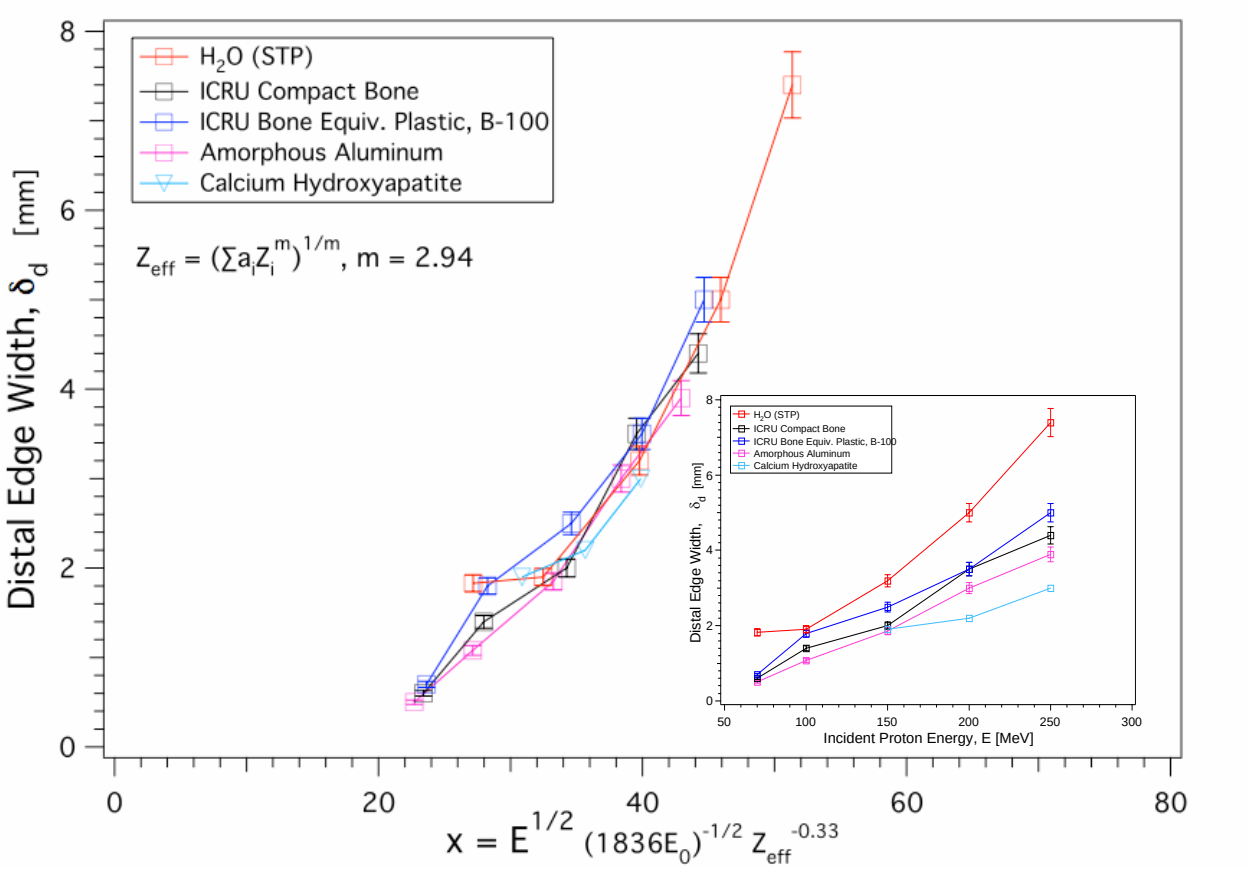

Figure III.2 Universal scaling of the distal edge width (distal penumbra) for homogeneous phantoms composed of five different materials. The material density ranges from 1 g/cm^3 for water to roughly 3.8 g/cm^3 for Calcium Hydroxyapatite, a common substitute for bone mineral. The inset shows the unscaled distal edge width for comparison

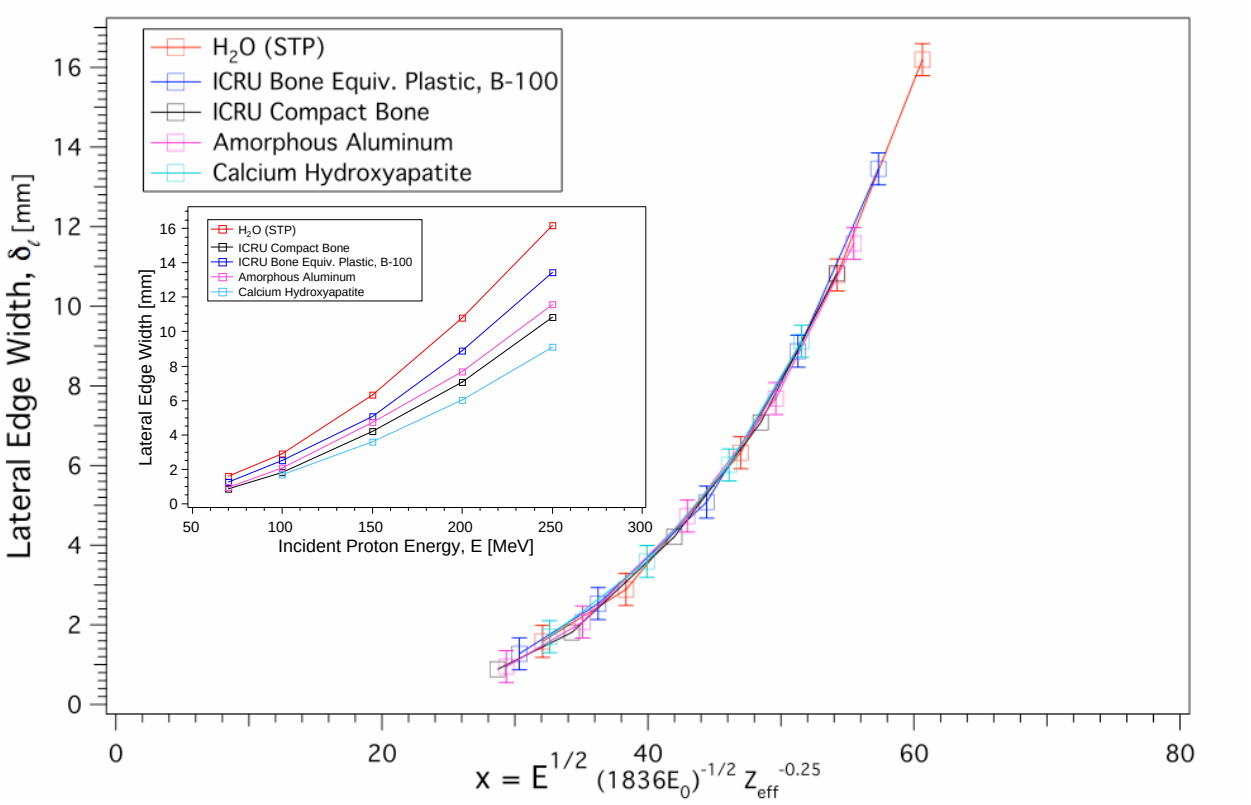

Figure III.3 Universal scaling of the lateral edge width (lateral penumbra). Phantom configuration is the same as for data in figure 2. Note that the exponent for Z_{eff} is 1/4 rather than 1/3 found for the distal edge width. The inset shows the unscaled lateral edge width for comparison.

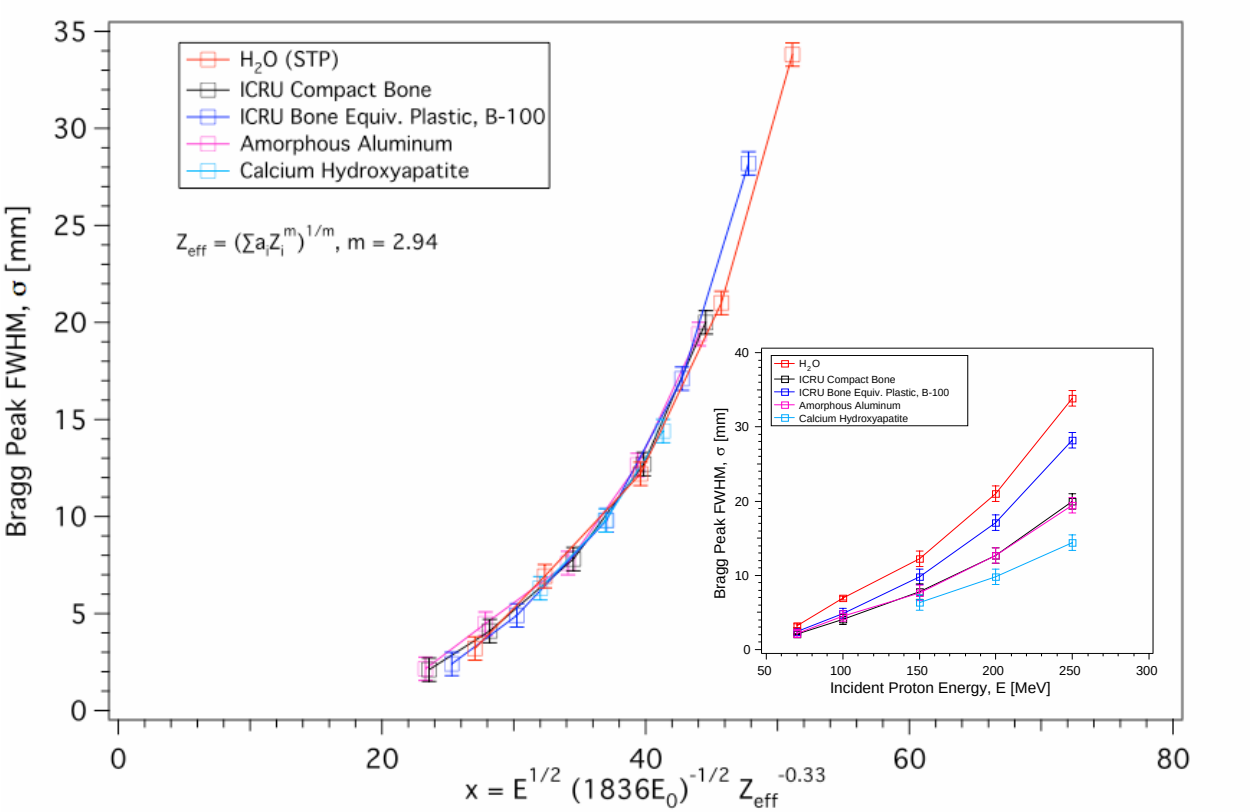

Figure III.4 Universal scaling of the Bragg peak FWHM. Phantom configuration is the same as for data in figure 2. The inset shows the unscaled FWHM for comparison.

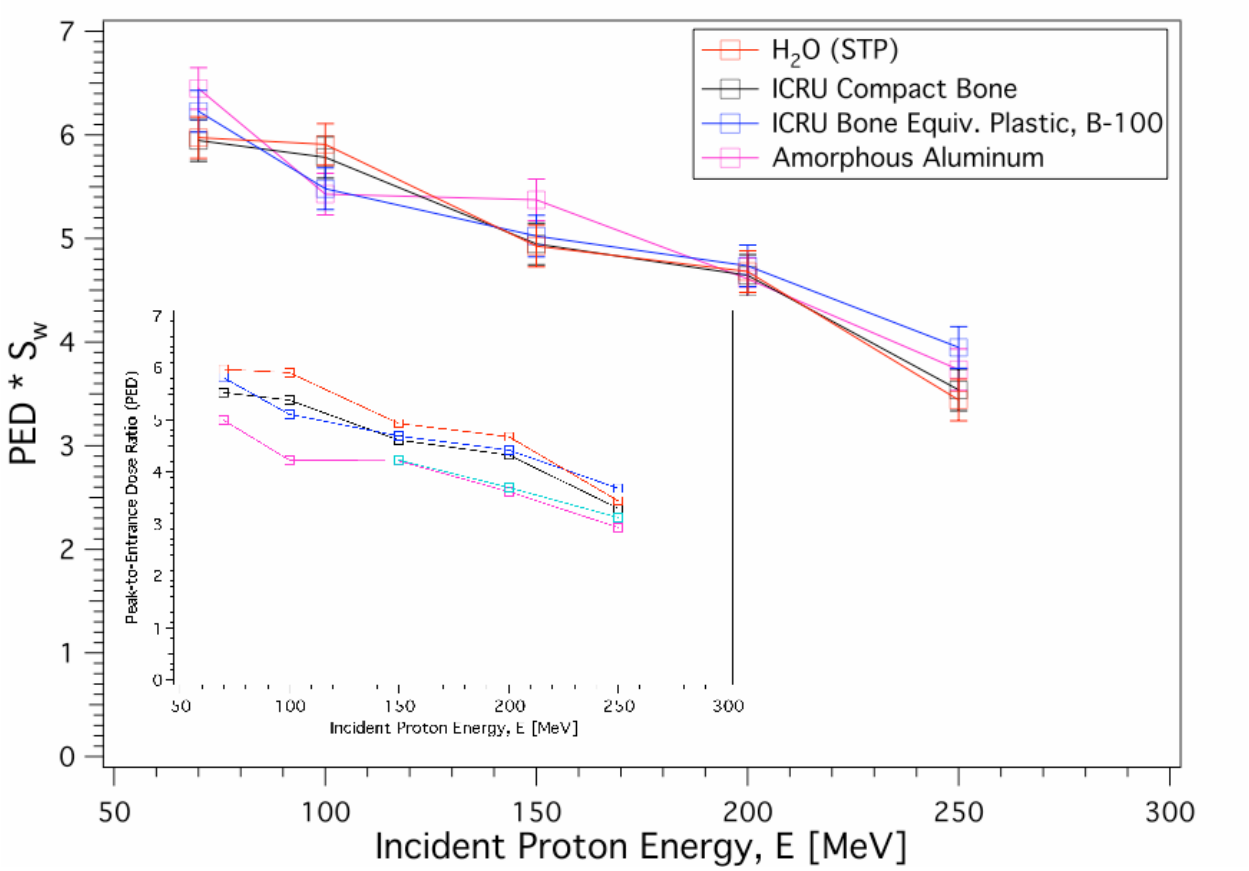

Figure III.5 Universal scaling of the Peak-to-Entrance Dose (PED) ratio. Phantom configuration is the same as for data in figure 2. Note here that the PED is not a spatial quantity and thus scaling with respect to the incident proton energy will fail. Instead the PED is directly scaled with the stopping power ratio.

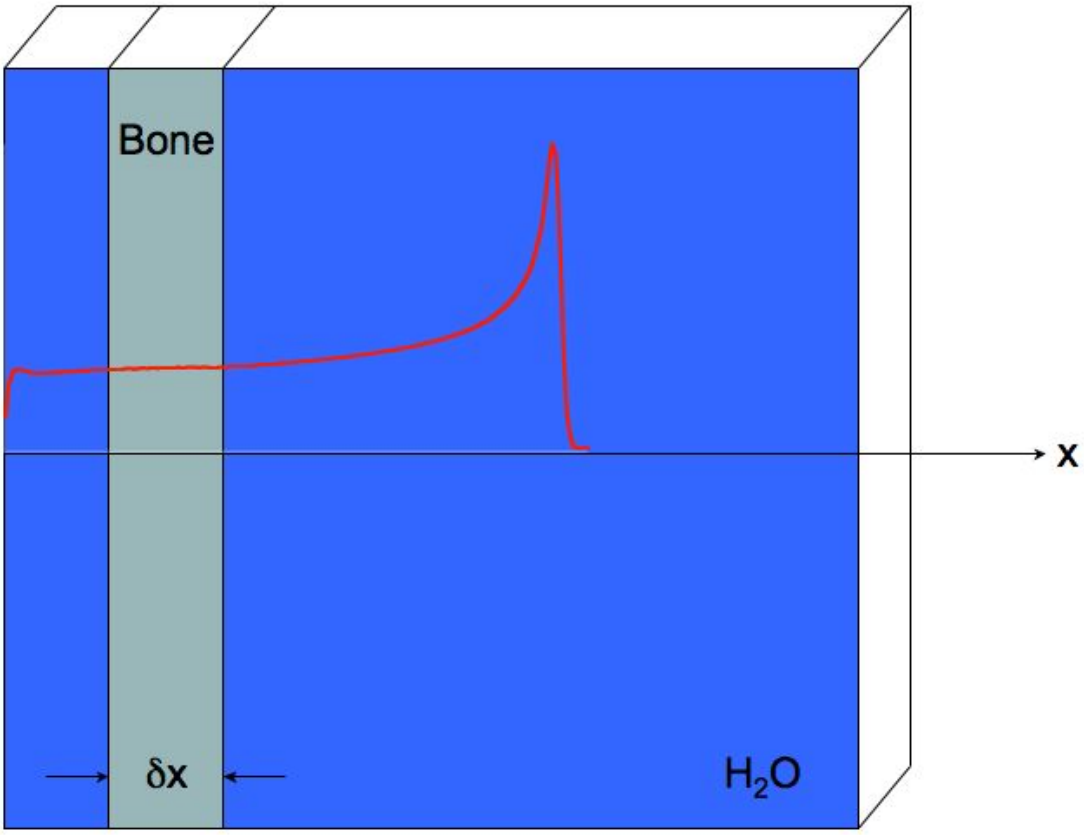

Figure III.6 Phantom layout including a single slab heterogeneity of compact bone. The red curve is an example of the Bragg curve for a single incident proton energy. The approximate relative distance between the bone slab the Bragg peak is shown. It was fixed such that even at the lowest energy of 70 MeV the peak resided well beyond the bone slab.

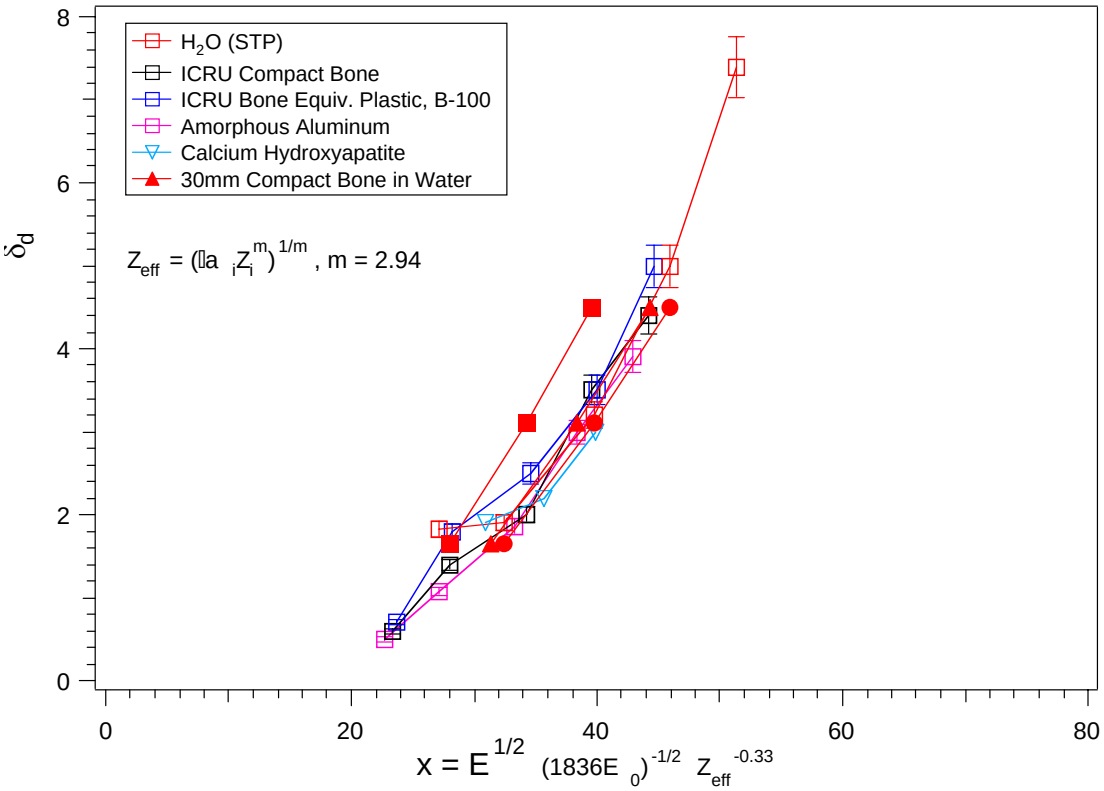

Figure III.7 Universal scaling of the distal edge width for homogeneous phantom configurations as shown in figure 2 as well as for a single bone/water heterogeneity. Note that scaling with the effective volume (defined in text) retains the universal scaling shown with Z_{eff}. The solid red squares are for the 30mm compact bone in water phantom but using the Z_{eff} of compact bone instead of from equation 4. The solid red circles are also for the heterogeneous phantom but with Z_{eff} of water instead of from equation 4.

Key Research Accomplishments

- Successfully adapted the GEANT4 code to read in DICOM-RT data so structures and beams could be transferred between a treatment planning system and the Monte Carlo program.
- Mapped the information in a CT dataset to a series of materials and densities so the Monte Carlo could accurately calculate doses on CT slices and construct DVHs from that data.
- Incorporated a realistic proton therapy nozzle, including modulator wheel and scattering system, into GEANT4.
- Began work on optimizing the spot-scanning delivery method including a comparison of optimization algorithms. Studied the effect of the distance between spots on the flatness of the resulting dose distribution.
- Began discussions with an MLC manufacturer regarding testing a prototype device.
- Presented work at the AAPM meeting in July 2005, the PTCOG meeting in December 2005, the APS meeting in March 2006. In addition Penn and WRAMC personnel attended the ATA meeting in San Diego in 2006.

Reportable Outcomes

The following abstracts based on work performed on this project have been accepted during the past year at scientific meetings:

1. Goulart D, Maughan R, McDonough J, Avery S**; "**Effects of Choice of the MLC Material On Neutron Dose Equivalent Outside of the Treatment Field in Proton Therapy"**.** AAPM meeting August 2006, Orlando FL.
2. Avery S, Goulart D, Maughan R, McDonough J; "4D Monte Carlo Simulation of a Commercial Proton Therapy Nozzle Using GEANT4 - Penumbra in Water". PTCOG43 meeting December 2005, Munich.
3. Avery S, Goulart D, Maughan R, McDonough J; "Analytical Neutron Shielding Calculations". PTCOG43 meeting December 2005, Munich.
4. Fry D, Sewchand W, O'Connell J; "An In-Depth Generic Characterization of Monte Carlo Generated Clinical Proton Depth-Dose". PTCOG43 meeting December 2005, Munich.
5. Fry D, Sewchand W, O'Connell J; "A Comparison of Three Monte Carlo Tools for Proton Radiotherapy: SRIM, PTRAN, and GEANT 4.7.0". PTCOG43 meeting December 2005, Munich.

Conclusions

This report documents the work that has been accomplished during the second year of the project to design an MLC for proton radiotherapy and the first year of work on the spot-scanning project. The next steps for the MLC project are to test electronics in a particle radiation field and to design and build a prototype. The

next steps in the spot scanning study are to improve the algorithm for static CT datasets then to move on to motion studies.

References

1. Slater JD, Yonemoto LT, Tossi CJ, et al.: "Conformal proton therapy for prostate carcinoma" Int J Radiat Oncol Biol Phys **42**:299-304, 1998.
2. Bush DA, Dunbar RD, Bonnet R, et al.: "Pulmonary injury from proton and conventional radiotherapy as revealed by CT" AJR **172**:735-739, 1999.
3. Isacsson U, Lennernas B, Grusell E, et al.: "Comparative treatment planning between proton and x-ray therapy in esophageal cancer" Int J Radiat Oncol Biol Phys **41**:441-450, 1998.
4. Miralbell R, Crowell C, Suit H: "Potential improvement of three dimension treatment planning and proton therapy in the outcome of maxillary sinus cancer" Int J Radiat Oncol Biol Phys **22**:305-310, 1991.
5. Slater JM, Slater JD, Archambeau JO: "Carcinoma of the tonsillar region: potential for use of proton beam therapy" Int J Radiat Oncol Biol Phys **22**:311-319, 1991.
6. Brown AP, Urie MM, Chisin R, et al.: "Proton therapy for carcinoma of the nasopharynx: a study in comparative treatment planning" Int J Radiat Oncol Biol Phys **19**:1607-1614, 1989.
7. Jakacki RI, Schramm CM, Donahue BR, Haas F, Allen JC, "Restrictive lung disease following treatment for malignant brain tumors: a potential late effect of craniospinal irradiation" Journal of Clinical Oncology. 13:1478-85, 1995.
8. Agostinelli S, et al, "GEANT4: A simulation toolkit", Nucl. Instrum. and Meth. **A506:**250-303 (2003).
9. Censor Y, Altschuler M D and Powlis W D "On the use of Cimmino's simultaneous projections method for computing a solution of the inverse problem in radiation therapy treatment planning" *Inverse Problems* **4** (1988).

Appendices

None